Simultaneous feedback control of plasma rotation and stored energy on NSTX-U using neoclassical toroidal viscosity and neutral beam injection

I. R. Goumiri,[1,a),b)] C. W. Rowley,[2] S. A. Sabbagh,[3] D. A. Gates,[4] M. D. Boyer,[4] S. P. Gerhardt,[4] E. Kolemen,[4] and J. E. Menard[4]
[1]*Department of Physics, University of Wisconsin, Madison, Wisconsin 53706, USA*
[2]*Department of Mechanical and Aerospace Engineering, Princeton University, Princeton, New Jersey 08544, USA*
[3]*Department of Applied Physics, Columbia University, New York, New York 10027, USA*
[4]*Princeton Plasma Physics Laboratory, Princeton, New Jersrey 08544, USA*

(Received 5 October 2016; accepted 21 November 2016; published online 23 February 2017)

A model-based feedback system is presented enabling the simultaneous control of the stored energy through β_n and the toroidal rotation profile of the plasma in National Spherical Torus eXperiment Upgrade device. Actuation is obtained using the momentum from six injected neutral beams and the neoclassical toroidal viscosity generated by applying three-dimensional magnetic fields. Based on a model of the momentum diffusion and torque balance, a feedback controller is designed and tested in closed-loop simulations using TRANSP, a time dependent transport analysis code, in predictive mode. Promising results for the ongoing experimental implementation of controllers are obtained. *Published by AIP Publishing.* [http://dx.doi.org/10.1063/1.4976853]

I. INTRODUCTION

The National Spherical Torus eXperiment Upgrade device NSTX-U,[1] which was completed in late 2015, is designed to make the previous device NSTX[2] the most powerful experimental fusion facility of its type in the world (spherical tokamak). Present experiments are testing the ability of the upgraded machine to maintain a high-performance plasma under conditions of high auxiliary heating power and relatively low magnetic field. Results could strongly influence the design of future fusion reactors like the fusion nuclear science facility FNSF,[3–5] by helping to understand some key physics issues such as non-inductively sustaining a plasma at high normalized beta, β_n.[6–11]

The two main components of the upgrade are the complete replacement of the NSTX-U center stack by 36 22-footlong, 350-pound copper conductors which contain the inner-leg of the toroidal field (TF) coils, the ohmic heating (OH) solenoid, and some divertor coils, and the addition of a second neutral beam injector, oriented more tangentially compared to the old set for NSTX. This will enable the temperature inside NSTX-U to exceed the 15×10^6 °C core of the sun, it will double the toroidal field (TF) capability reaching about 1.0 T, and will also double the plasma current reaching about 2.0 MA.

The high-performance operational goals of NSTX-U require the development and the extension of advanced feedback control algorithms based on the successful advances made on NSTX to the upgraded device, including the control of β_n,[12] plasma boundary shape,[13,14] current[15] and rotation[16] profiles, and edge transport barrier.[17] Major advancements in plasma control will be essential to help scientists achieving some important NSTX-U experimental goals, and work has already been undertaken to upgrade the hardware and software of the plasma control system (PCS) for NSTX-U,[18] and to develop the new control algorithms needed to optimally handle the complete complex dynamics of the system: addressing a far greater range of global parameter and profile control.

Toroidal rotation has been shown to have an important effect on MHD instabilities where altering the plasma profile and speed can increase the stability of tearing, kink/ballooning, and resistive wall modes.[19–23] Therefore, we will control the toroidal rotation along with plasma normalized beta to maintain plasma stability which is an important factor towards avoiding disruptions in tokamaks: a loss of the plasma stored energy or a change in rotation profile can cause severe damages inside the vessel of the device.

One of the many causes of disruption is the increasing of the plasma pressure. The plasma pressure is typically normalized by the toroidal magnetic field strength B_T. It is denoted by β_T and is equal to $\beta_T = 2\mu_0\langle P\rangle/B_T^2$ where $\langle P\rangle$ is the volume averaged total pressure, and μ_0 is the permeability of free space. However, this toroidal β_T is not a good indicator of proximity to instability,[24] a typical parameter used to determine plasma stability is the normalized beta β_N which is given by $\beta_N = 10^8 a B_T \beta_T / I_P$ where I_P is the plasma current, and a is the minor radius (MKS units). β_N and plasma rotation profile are the desired controllable quantities in order to operate safely, the near stability boundaries by avoiding disruption and enabling other parameters to vary while β_N is kept fixed.[12]

The importance of the stored energy control has been shown by the implementation of β_N control system on several tokamaks: DIII-D,[25] TFTR,[26] JET,[27] and NSTX.[9,12] Another work in this area has been done at JT-60-U, where a functional parameterization method was used to calculate the stored energy in real time.[28] Further work on DIII-D[29] have extended these studies to simultaneous control of β_N and

Note: Paper BI2 5, Bull. Am. Phys. Soc. **61**, 22 (2016).
[a)]Invited speaker.
[b)]goumiri@wisc.edu

plasma rotation using the capability provided by having both counter and co-injecting neutral beams.

In this paper, a new approach to simultaneously control the toroidal rotation profile and β_n is proposed for NSTX-U. It is similar to the DIII-D work[29] but has a different variation of the total beam power and the three dimensional magnetic field coil current (different set of actuators). Although rotation control based on data driven models has been studied for NSTX,[16] in the present work, we make the important addition of greatly extending the rotation profile control range by including twice as many neutral beam sources (more actuators) with a much broader momentum deposition, and the ability to simultaneously control the plasma β_n.

Since NSTX-U experimental data is not yet available, the robustness of our controller in terms of stability and performance will be assessed to predict its limits when the energy confinement time (τ_E) and the momentum diffusivity coefficient (χ_ϕ) vary. The dynamical models for the stored energy and rotation profile will be identified from numerical simulations generated using predictive TRANSP, a time dependent plasma transport analysis code simulations (methods for system identification can later be applied to experimental data).

TRANSP[30,31] will enable high-fidelity testing of a variety of control algorithms, while reducing the amount of expensive experimental time needed to implement new control algorithms on NSTX-U or other devices.

This paper is organized as follows. Section II describes the (extrapolated-)data driven model with details about the actuators used, the model reduction process and a comparison to different TRANSP predictions. Section III describes briefly the optimal control method used to track a desired rotation profile and a desired stored energy, using both neoclassical toroidal viscosity (NTV) and neutral beam injection (NBI) as actuators, and its implementation through numerical simulation. Section IV presents the results of controlling a more complete rotation and energy model through TRANSP. Conclusions and future work are discussed in Section V.

II. A SIMPLIFIED MODEL OF THE TOROIDAL MOMENTUM AND STORED ENERGY BALANCE

A. Model definition

The modeling consists of two coupled equations: one for the transport of toroidal angular plasma momentum in a tokamak with the assumption of axisymmetry, the other one for its corresponding stored energy. An arbitrary flux surface average $\rho \in [0, 1]$ is used, where $\rho = 0$ and 1 denote the center and the boundary of the plasma, respectively.

Based upon the work by Goldston[32] and Callen,[33] the angular velocity of the plasma ω can be described dynamically by the flux surface average $\langle\cdot\rangle$ of a simplified version of the toroidal momentum equation[16]

$$(nm)\langle R^2\rangle \frac{\partial \omega}{\partial t} = \left(\frac{\partial V}{\partial \rho}\right)^{-1} \frac{\partial}{\partial \rho}\left[\frac{\partial V}{\partial \rho}(nm)\chi_\phi \langle R^2(\nabla\rho)^2\rangle \frac{\partial \omega}{\partial \rho}\right] + \sum_{i=1}^{4} T_{\mathrm{NBI}i} + T_{\mathrm{NTV}}, \quad (1)$$

with boundary conditions

$$\left.\frac{\partial \omega}{\partial \rho}\right|_{\rho=0} = 0 \quad \text{and} \quad \omega|_{\rho=1} = 0. \quad (2)$$

This Dirichlet boundary condition at the plasma edge is chosen to be consistent with NSTX experimental observations. The left-hand side of Equation (1) represents the temporal change in the plasma toroidal angular momentum and the right-hand side terms denote respectively the viscous dissipation term, and the torque inputs from neutral beam injection (NBI) and neoclassical toroidal viscosity (NTV). R is the major radius, $\partial V/\partial\rho$ is the differential flux surface volume, and χ_ϕ is the perpendicular (to the equilibrium magnetic field) momentum diffusivity. n is the particle density, and m is the particle mass. For simplicity, only the main plasma ion species is considered in the dynamics. $T_{\mathrm{NBI}i}$ and T_{NTV} represent the neutral beam and neoclassical toroidal viscosity torques respectively. Full details of these models are shown in Section II B 1.

TRANSP evolves the stored energy by heat and particle diffusion equations but for simplicity, the model of the total plasma stored energy W is given by the following equation:

$$\frac{\partial W}{\partial t} + \frac{W}{\tau_E} = \sum_{i=1}^{4} P_{\mathrm{NBI}i}(t), \quad (3)$$

where $P_{\mathrm{NBI}i}$ represents the beam power from four modeled sources, the first source will be the simplified model of the initial NSTX set of beams as its footprints are similar, the three other sources will correspond individually to the upgraded set of beams (NSTX-U). τ_E represents the energy confinement time, which is modeled by an ITER 98 empirical energy confinement scaling[34] given by

$$\tau_E = H_{98y,2} 0.0562 I_P^{0.93} B_T^{0.15} n_e^{0.41} P_{Loss(th)}^{-0.69} R_0^{1.97} \epsilon^{0.58} \kappa^{0.78}, \quad (4)$$

where I_P is the plasma current, B_T is the toroidal magnetic field, n_e is the line-averaged electron density, R_0 is the major radius, ϵ is the inverse aspect ratio, and κ is the elongation. The loss power $P_{Loss(th)}$ is defined as the total input heating power less $\frac{\partial W}{\partial t}$ and fast ion losses through charge-exchange, bad orbits, and shine-through.[35] $H_{98y,2}$ is a constant.

Figure 1 shows a TRANSP simulation of plasma discharge 142301X for NSTX-U device compared to a reconstructed data from a plasma discharge of NSTX (133367). The first quantities are time averaged (black lines) for NSTX-U, the other ones (blue lines) are chosen to be fixed values at an adequately chosen time ($t = 0.65$ s) for NSTX. Except for the density which is higher for NSTX-U due to the additional effect of the three new neutral beam injections, there is not much difference between these geometrical quantities in the two devices. Note that 142301X is not a real or a reconstructed shot. It is an extrapolated simulation obtained through predictive TRANSP, it relies heavily on the NSTX data analysis extrapolated to a possible NSTX-U scenario.

Figure 2 shows the deduced χ_ϕ from the same NSTX-U run (plasma simulation number 142301X) compared to a

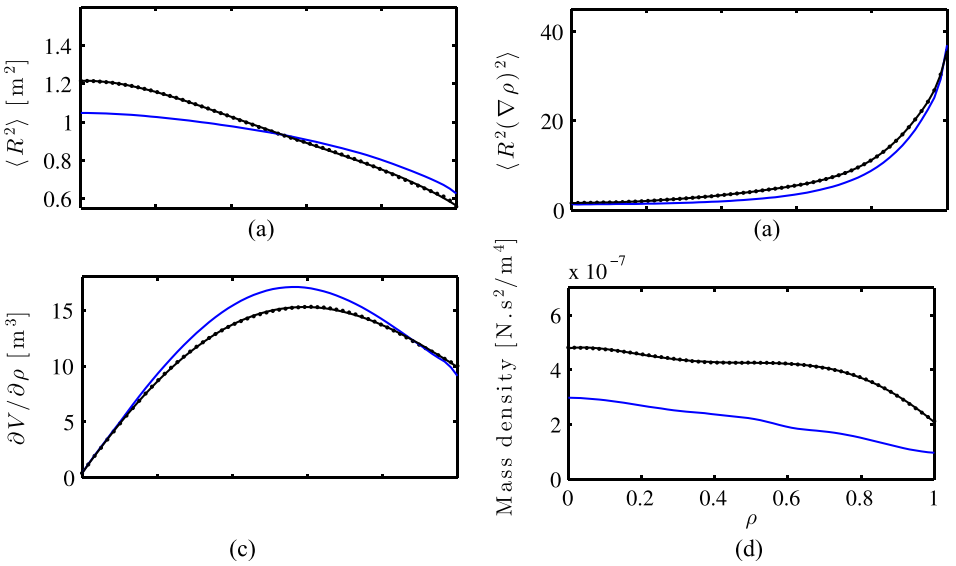

FIG. 1. Functions describing the radial profiles of the geometrical properties: $\langle R^2 \rangle$, $\langle R^2(\nabla\rho)^2 \rangle$, $\partial V/\partial\rho$, and the mass density nm from a TRANSP simulation of plasma discharge 142301X (NSTX-U). In blue, the same corresponding functions for TRANSP analysis of plasma discharge 133367 (NSTX) are shown for comparison. The time-average values are shown by the black dots, and its curve-fits are shown by the black lines respectively.

model taken from the NSTX discharge 133367. The model based system will use the χ_ϕ of discharge 142301X as its momentum diffusivity coefficient reference. In this NSTX-U scenario, the plasma current has been doubled as a reasonable extrapolation. It implies that the energy confinement time τ_E doubles too, and because this latter scales the same as the momentum diffusion time, it is reasonable to argue that the NSTX-U momentum diffusivity χ_ϕ would roughly be half of the NSTX χ_ϕ model.

Some observations can be made about this coupled simplified model: Equation (1) is parabolic, this ensures that the system is stable (desirable feature for control). Equation (3) is a first order ordinary differential equation (ODE) that links directly the stored energy to the beam power actuators. Its steady state depends on the energy confinement time.

The two important parameters in the modeling are the diffusion coefficient χ_ϕ and the energy confinement time τ_E which are considered to be constant in time in Equations (1) and (3) respectively. There are no direct measurements of χ_ϕ nor τ_E inside the tokamak, but TRANSP is able to reconstruct the value for the χ_ϕ parameter for a simulation where ω is given (simulated), and the modeling of τ_E has already been encapsulated inside TRANSP through the Expert file code (more details in Boyer *et al.*[15]).

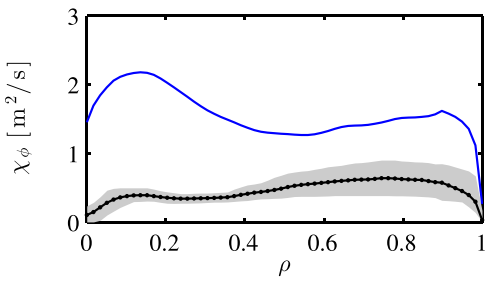

FIG. 2. The momentum diffusivity coefficient χ_ϕ is calculated through TRANSP simulation of plasma discharge 142301X. The shaded region represents the value of the function spanned over time interval (4–6) s. In blue, the same corresponding quantity for TRANSP analysis of plasma discharge 133367 (NSTX) is shown for comparison. The time-average values and its curve-fit are shown by the black dots and the solid black line respectively.

The strategy for constructing a controller based on the equations above is as follows: given a range of desired profiles of toroidal rotation and stored energy values that the operator wants the system to reach and stabilize around, take the simplified model (1–3), linearize it around an equilibrium whose basin of attraction contains the range of desired profiles and values and then apply model reduction before designing a controller that will attempt to match any target shape within this range.

Because of the lack of experimental data, a full robustness study of stability and performance of the designed controller when uncertainties occur on certain parameters of the model will be presented in Section III D as a consolidation of our controller design.

B. Actuator models

In NSTX-U, neutral beam injection is the main method considered here to produce a positive torque to increase plasma rotation, which is achieved by injecting high-speed neutral atoms into the plasma.

Figure 3 shows the neutral beam injection for the present upgrade of NSTX.

1. Neutral beam injection (NBI)

The main difference between NSTX and NSTX-U is the increase of the number of actuators from one (three neutral beams modeled as a single one for simplification due to similarities in their profile) to four actuators which consist of the addition of the three new beam sources. These new beams are considered individually because unlike in the previous setting of NSTX, the new set of beams is oriented more tangentially. Similarly to Goumiri *et al.* work,[16] we start by modeling the NBI torques as a product of the spatial average of the torques, $\bar{T}_{\mathrm{NBI}_i}(t) \equiv \mathrm{avg}_\rho T_{\mathrm{NBI}_i}(t,\rho)$, and a function, $F_{\mathrm{NBI}_i}(\rho)$, that represents the spatial profile. We then have for $i = 1, \ldots, 4$

$$T_{\mathrm{NBI}i}(t,\rho) = \bar{T}_{\mathrm{NBI}_i}(t) F_{\mathrm{NBI}_i}(\rho). \tag{5}$$

Figure 4 represents the footprints $F_{\mathrm{NBI}i}$ of the six beam powers involved in the actuation. We can notice that the first set

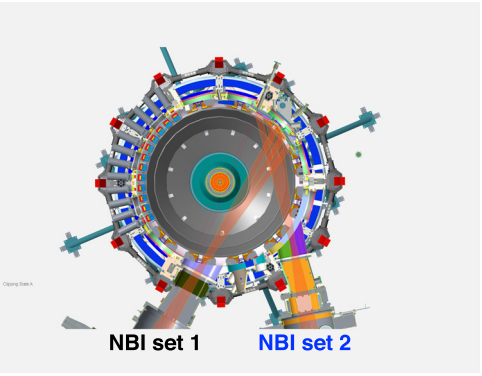

(a)

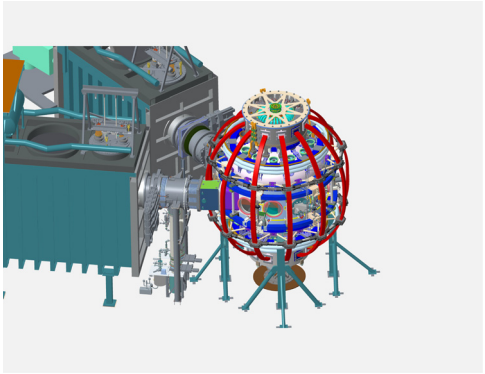

(b)

FIG. 3. Illustration of the neutral beam injection (NBI) devices for NSTX-U with an inside view from the top of the tokamak (top) and outside view (bottom).

of beam has a similar profile (the three grey dash lines) which is high at the core of the plasma and low towards the edge. For simplicity, it will be modeled by a Gaussian function (red solid line in Figure 4) written as

$$F_{\mathrm{NBI}_1}(\rho) = a_{\mathrm{NBI}} \exp\left(-\frac{\rho^2}{2\sigma_{\mathrm{NBI}}^2}\right), \tag{6}$$

where the parameters $a_{\mathrm{NBI}} = 4.8212$ and $\sigma_{\mathrm{NBI}} = 0.2219$ are determined by a least-squares fit to the time-averaged data for NSTX. We have kept the same modeling for the first beam set as the one done in Goumiri *et al.*[16] We notice also that the footprints of the beam power of the second set are more spread out along the plasma, with some high peaks toward the middle of the plasma. This enables us to vary the location of actuation of the beam power which allows better control. This latter set of profiles is kept as it is and treated individually.

The time dependency of the NBI torque $\bar{T}_{\mathrm{NBI}}(t)$ is governed by the power input, $P_{\mathrm{NBI}i}$ through a first-order lag

$$\frac{\partial \bar{T}_{\mathrm{NBI}i}}{\partial t} + \frac{\bar{T}_{\mathrm{NBI}i}}{\tau_{\mathrm{NBI}i}} = \kappa_{\mathrm{NBI}i} P_{\mathrm{NBI}i}(t), \tag{7}$$

for $i = 1, \ldots, 4$, where $\tau_{\mathrm{NBI}i}$ are the slowing down times of the fast neutral beam particles to impart energy to the bulk plasma, and $\kappa_{\mathrm{NBI}i}$ are scalars used to normalize the neutral beam powers $P_{\mathrm{NBI}i}$.

Figure 5 shows the solution of Equation (7) with only P_{NBI2} fixed to 2 MW, compared with the neutral beam torque predicted by TRANSP analysis, which uses a more elaborate Monte Carlo model (beam A of the second set). It can be noticed that by choosing the parameters (τ_{NBI} and κ_{NBI}) adequately, the $\bar{T}_{\mathrm{NBI}}$ model captures very well, the TRANSP simulation of this torque. The same procedure will be applied to the rest of the time dependent NBI torques (beams B and C of the second set of beams of NSTX-U).

2. Neoclassical toroidal viscosity (NTV)

Neoclassical toroidal viscosity (NTV) is a physical effect caused by the non-ambipolar diffusion of ions and electrons.[36] The effect can be created by the application of non-axisymmetric fields in a tokamak, and has been demonstrated to provide an actuator for plasma rotation in NSTX.[37] Depending on the spectrum of the non-axisymmetric field applied, NTV can be created over significant portions of the plasmas. Application of fields that are largely non-resonant with MHD modes (e.g., toroidal mode number of three) allow fine control of the plasma rotation in the region of strong NTV by changing the coil currents producing the field.

For the current one-dimensional toroidal momentum model, modeling the momentum loss due to the neoclassical toroidal viscosity will be based on the work done in Zhu *et al.*[37] from which we can design the NTV torque as the bilinear product of the coil current squared (I^2) with the toroidal momentum ω as follows:

$$T_{\mathrm{NTV}}(t, \rho) = K\, G(\rho)\, \langle R^2 \rangle\, I^2(t)\, \omega(t, \rho), \tag{8}$$

where K is a constant, and G is a Gaussian function centered towards the edge ($\mu = 0.7, \sigma = 0.1$). The control actuator input will be the coil current $I(t)$.

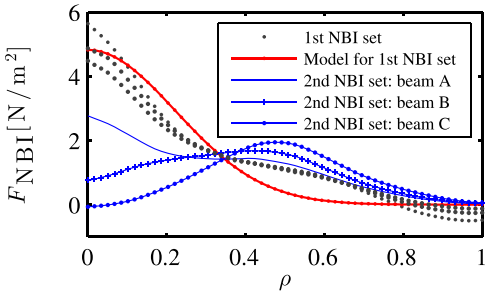

FIG. 4. Spatial profile for the neutral beam torque (F_{NBI}) for plasma simulation 142301X.

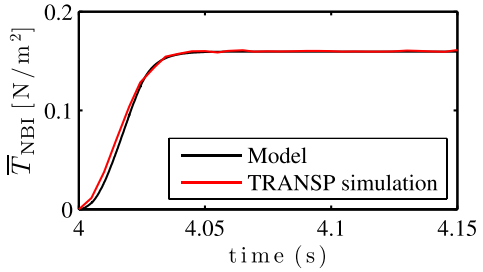

FIG. 5. Time dependent profile for the neutral beam torque ($\bar{T}_{\mathrm{NBI}}$) for plasma simulation 142301X. (second NBI set, beam A) with $\tau_{\mathrm{NBI}} = 0.008$ s and $\kappa_{\mathrm{NBI}} = 9.8 \times 10^{-6}$.

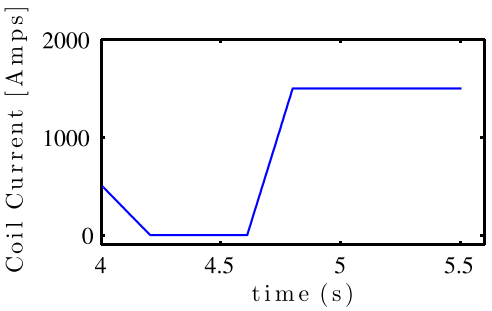

FIG. 6. Coil current I(t) for plasma simulation 142301X model.

Figure 6 shows a model of current that flows into the coils for a plasma simulation.

Figure 7 shows a numerical model of the 3D magnetic coils that is wrapped around the NSTX-U tokamak and used to create the three dimensional field.

Figure 8 represents the T_{NTV} torque where the given coil current I shown in Figure 6 and ω modeled from TRANSP predictive simulation 142301X are combined. We can notice that the peak of the NTV torque (towards the edge) overlaps with the peaks of the second set of NBI torques. This would create regions where a drag (NTV) and a drive (NBI) are applied simultaneously.

A direct consequence of the coexistence of opposite actuators is that while calculating the feedforward values of inputs (coil current and beam power) necessary for the tracking problem, several solutions do exists for the same desired profile, and some of these solutions do not respect the physical constraints (threshold limits) imposed on the inputs. A solution to overcome this issue will be presented in the controller design in Section III.

C. Testing and comparing the model

1. Discretization of the model

In order to numerically simulate the partial differential equation (1), we use a spectral method, projecting onto

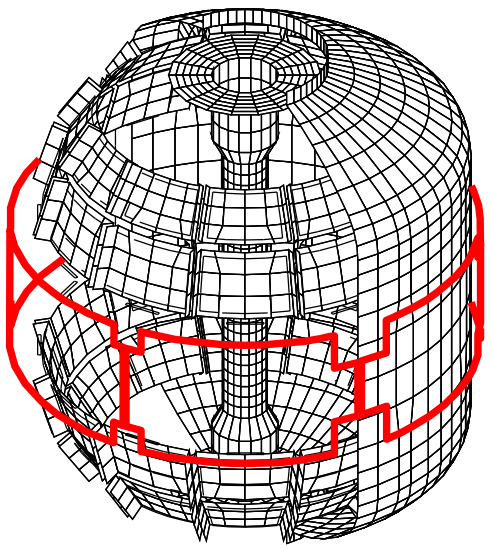

FIG. 7. Model of the three-dimensional coils (highlighted in red) used to create the magnetic field that produces NTV in the NSTX-U device.

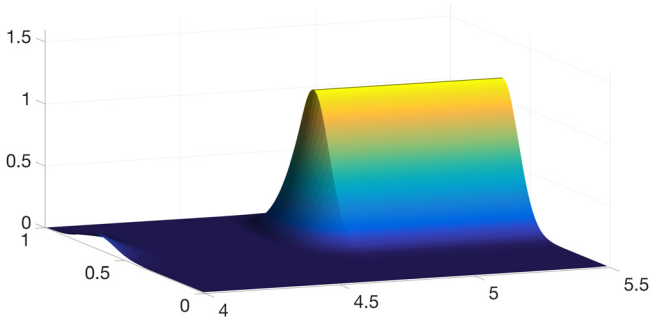

FIG. 8. 3D representation of the NTV torque model (8) where ω is taken from TRANSP prediction simulation of 142301X, and current I is as shown in Figure 6.

suitably chosen basis functions, to obtain a system of ordinary differential equations. Therefore the rotation profile can be rewritten as

$$\omega(\rho,t)=\sum_{n=1}^{N}a_n(t)\varphi_n(\rho), \tag{9}$$

where the basis functions are given by

$$\varphi_n(\rho)=J_0(k_n\rho),\quad n=1,\ldots,N, \tag{10}$$

where J_0 denotes the Bessel function of the first kind, and k_n denotes the n-th root of J_0.

Note that (1) is linear in ω, and can be written as

$$\partial\omega/\partial t=L(\omega,T_{\mathrm{NBI}},T_{\mathrm{NTV}}), \tag{11}$$

where L is a differential operator linear in each argument. After some manipulation, Equation (11) simplifies into

$$\dot{a}_m=\sum_{n=1}^{N}\frac{\langle L(\varphi_n,T_{\mathrm{NBI}},T_{\mathrm{NTV}}(\varphi_n)),\varphi_m\rangle}{\langle\varphi_m,\varphi_m\rangle},\quad m=1,\ldots,N, \tag{12}$$

which is a set of N coupled ordinary differential equations for the coefficients a_m.

Equation (3) is considered as a scalar ODE equation which will be added to the projected rotation equation as an additional line in the matrix form.

2. Comparison model vs. TRANSP simulation

The parameters in the model (1) are determined from the TRANSP predictive model of plasma discharge 142301X, as mentioned in Section II.

Figure 9 represents the comparison of the model vs. the TRANSP analysis (prediction of plasma scenario 142301X) when all beams are activated combined with the NTV torque deduced from the coil current defined in Figure 6.

Figure 10 represents the same information as Figure 9 but with a different coil current model. We can notice that $N=8$ Bessel modes capture the main features of the dynamics for relative errors of about 25%. The overall behavior of the plasma is captured qualitatively very well using the simplified model of Equation (1) with a fixed (averaged) background.

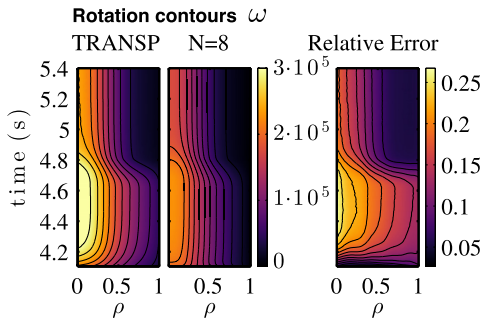

FIG. 9. Comparison of the rotational frequency ω for a plasma simulation using the coil current shown in Figure 6, comparing TRANSP prediction with the simplified model projected onto $N=8$ Bessel modes. Also shown is the relative error between TRANSP and the reduced model ($N=8$).

We rely exclusively on model based dynamical predictions. Feedback control will be performed and designed to tolerate errors in the model, and its robustness to stability and performance will be studied by modeling the uncertainties of the model by some intervals of variation of model parameters. We will ensure that the designed controller will reach its objectives within this range of variations.

III. LINEAR PLASMA ROTATION CONTROL

The purpose of this section is to demonstrate that standard model-based control techniques may be used to guide a future experimental plasma rotation profile to track a desired reference.

Recall that the actuators available to the controller are the (NBI) beam power and the coil current producing NTV. In this case, a state-space realization is derived and linear quadratic regulators are used to design a feedback controller that is optimal in minimizing a prescribed quadratic cost function.

A. State space realization

The goal is to rewrite our original simplified nonlinear system as a linearized state space realization, in order to use the appropriate linear control tools on it.

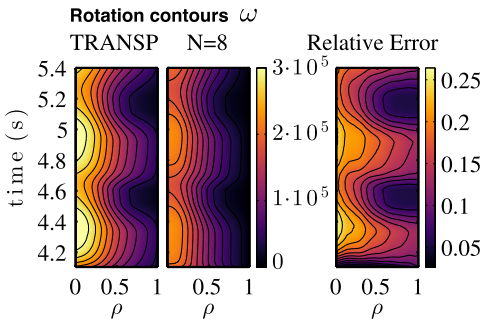

FIG. 10. Comparison of the rotational frequency ω for a plasma simulation using a different coil current, comparing TRANSP prediction with the simplified model projected onto $N=8$ Bessel modes. Also shown is the relative error between TRANSP and the reduced model ($N=8$).

Let $\bar{\omega}$ and $\bar{W}$ be the steady state reached for the given $\bar{P}_i$ and current $\bar{I}$. The linearization around this given steady state profile can be written as

$$\omega(t,\rho) = \bar{\omega}(\rho) + \omega'(t,\rho), \tag{13}$$

$$W(t) = \bar{W} + W'(t), \tag{14}$$

$$I(t) = \bar{I} + I'(t), \tag{15}$$

$$P_{\mathrm{NBI}i}(t) = \bar{P}_i + P'_i(t), \tag{16}$$

where ω', W', I', and P'_i are the respective perturbations to the equilibria $\bar{\omega}$, $\bar{W}$, $\bar{I}$, and $\bar{P}_i$. By plugging in these equations into Equations (1), (3), (5), and (8) then simplifying, we obtain

$$\frac{\partial}{\partial t}\begin{bmatrix}\omega'\\ \bar{T}_1\\ \bar{T}_2\\ \bar{T}_3\\ \bar{T}_4\\ W'\end{bmatrix} = \begin{pmatrix} a_{11} & a_{12} & a_{13} & a_{14} & a_{15} & 0\\ 0 & a_{22} & 0 & 0 & 0 & 0\\ 0 & 0 & a_{33} & 0 & 0 & 0\\ 0 & 0 & 0 & a_{44} & 0 & 0\\ 0 & 0 & 0 & 0 & a_{55} & 0\\ 0 & 0 & 0 & 0 & 0 & a_{66}\end{pmatrix}\begin{bmatrix}\omega'\\ \bar{T}_1\\ \bar{T}_2\\ \bar{T}_3\\ \bar{T}_4\\ W'\end{bmatrix} + \begin{pmatrix} b_{11} & 0 & 0 & 0 & 0\\ 0 & b_{22} & 0 & 0 & 0\\ 0 & 0 & b_{33} & 0 & 0\\ 0 & 0 & 0 & b_{44} & 0\\ 0 & 0 & 0 & 0 & b_{55}\\ 0 & 1 & 1 & 1 & 1\end{pmatrix}\begin{bmatrix}I'^2\\ P'_1\\ P'_2\\ P'_3\\ P'_4\end{bmatrix}, \tag{17}$$

where

$$\begin{aligned} a_{11} &= \frac{1}{nm\langle R^2\rangle}\left(\frac{\partial V}{\partial\rho}\right)^{-1}\frac{\partial}{\partial\rho}\left[\frac{\partial V}{\partial\rho}(nm)\chi_\phi\langle R^2(\nabla\rho)^2\rangle\frac{\partial}{\partial\rho}\right] \\ &\quad -\frac{1}{nm}KG(\rho)I_0^2 \\ a_{1,i+1} &= \frac{F_{NBI_i}(\rho)}{nm\langle R^2\rangle} \\ a_{i+1,i+1} &= -\frac{1}{\tau_{NBI_i}} \\ a_{6,6} &= -\frac{1}{\tau_e} \\ b_{11} &= -\frac{1}{nm\langle R^2\rangle}KG(\rho)\langle R^2\rangle\omega_0 \\ b_{i+1,i+1} &= \kappa_{NBI_i}. \end{aligned}$$

Equation (17) is the state-space realization needed for the linear control design.

Let $x = (a_0, a_1, \ldots, a_r, \bar{T}_1, \bar{T}_2, \bar{T}_3, \bar{T}_4, W')$ be the $(r+1)$ Bessel coefficients of the projection of the partial state ω on the r chosen Bessel functions combined with the four time dependent torques and the scalar thermal energy. Let $u = (I'^2, P'_1, P'_2, P'_3, P'_4) \in \mathbb{R}^p$ be the perturbed input, and $y \in \mathbb{R}^q$ be the perturbed output (sensor measurements from their

equilibrium values). This system of equations can be represented in the standard state-space form

$$\dot{x} = Ax + Bu, \tag{18}$$

$$y = Cx, \tag{19}$$

by using the spectral decomposition described in Section II C. $A \in \mathbb{R}^{(r+6)\times(r+6)}$, $B \in \mathbb{R}^{(r+6)\times p}$, and $C \in \mathbb{R}^{q\times(r+6)}$ are respectively called the dynamics, control, and sensor matrices. Here, there are five actuators ($p = 5$), four power input for the neutral beams and another one for the coil current producing the NTV. The outputs y correspond to the sensor measurements of the plasma toroidal rotation. Here, five measurements are taken, spread from the core towards the edge of the plasma ($q = 5$).

Scaling plays a very important role in our application: it simplifies the model analysis and the controller design (weight selection). In order to do that, expected magnitudes of the disturbances and reference changes on the magnitude of each input $(I'^2, P'_1, P'_2, P'_3, P'_4)$ and output $(\omega_1, \omega_2, \omega_3, \omega_4, W)$ signal has to be known respectively. After a matrix manipulation, we obtain the following scaled linear model:

$$\dot{\hat{x}} = \hat{A}\hat{x} + \hat{B}\hat{u}, \tag{20}$$

$$\hat{y} = \hat{C}\hat{x}, \tag{21}$$

where $\hat{(\cdot)}$ is used for scaled quantity. From this point on, without loss of generality, we will always refer to the scaled quantities and omit the $\hat{(\cdot)}$ signs.

B. Non-zero target state

The purpose here is to force the shape of the plasma rotation profile and thermal energy to reach a target state x_d such that the sensor output y matches a reference signal y_d. In the final implementation, all one should have to prescribe is y_d (e.g., plasma rotational frequency values at certain locations and the desired thermal energy). The target state x_d and the corresponding input u_d are found by solving Equations (20) and (21) at steady state ($\dot{x} = 0 = Ax_d + Bu_d$ and $y_d = Cx_d$). We then solve for x_d and u_d by writing in matrix form

$$\begin{pmatrix} x_d \\ u_d \end{pmatrix} = \begin{pmatrix} A & B \\ C & 0 \end{pmatrix}^{-1} \begin{pmatrix} 0 \\ I \end{pmatrix} y_d = \begin{pmatrix} F_x \\ F_u \end{pmatrix} y_d. \tag{22}$$

While this solution is mathematically valid and unique, it may lead to solutions that violate the physical limitations of our actuators. An approximate solution which respects our actuator constraints is thus required. Intuitively, since both a drag (NTV torque) and a drive (NBI torque) are present in the middle of the plasma, it is clear that there are multiple approximate solutions. We use convex optimization to solve for x_d and u_d while respecting our actuator constraints. More details can be found in Refs. 38 and 39.

Figure 24 defines our initial profile, the equilibrium profile used for the linearization and the targeted profile where the measurements are done.

The location of existing sensors on NSTX has not been carefully chosen with rotation control in mind. A good positioning of sensors maximizes the ratio of the magnitude of measured outputs to inputs. Conveniently, this ratio is comprised between the smallest and the largest singular values of the system (Equations (20) and (21)) which are easy to compute at any frequency. Furthermore, since we are mostly interested in the steady-state solution, it is enough to compute them at frequency 0 rad/s. With just 4 sensors located at 4 distinct locations on a coarse discretization of the radial variable, we simply use brute-force to find the optimal arrangement such as to maximize the average value of this ratio, that is, the average of the singular values of the system.

C. Control design

Once the target states (x_d, u_d) are established, the controller is designed based on the reduced model dynamics, and then applied to the full-dimensional linearized model, and finally tested on the original nonlinear model to determine if the controller can suppress disturbances and reach the desired rotation profile and thermal energy value at the same time, in the vicinity of the equilibrium.

Figure 11 represents the schematic of the controller design. It has five main components:

1. Feedforward design

From the set of measurements of the desired rotation profile and thermal energy combined in the vector y_d, the feedforward gain converts it into the desired state x_d and input u_d needed in order to reach the target.

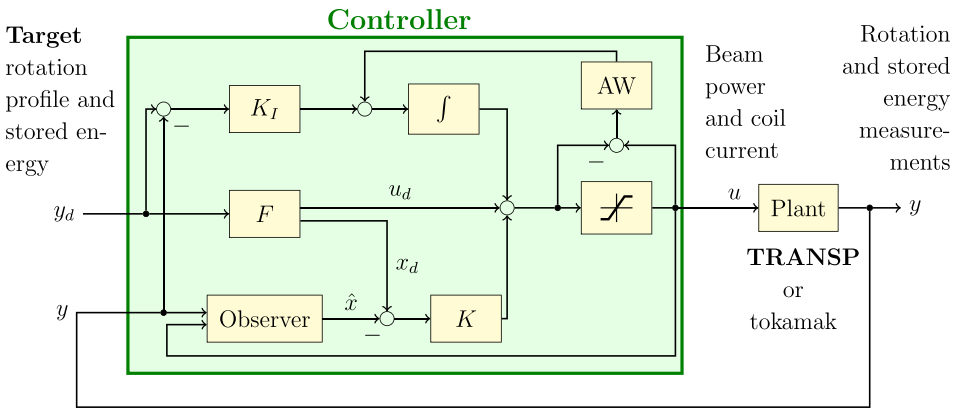

FIG. 11. Global schematic of the controller that combines a feedforward (F), a LQR (K), an observer, an integrator (K_I), and an anti-windup (AW).

If the model of the dynamics has no errors or uncertainties (which is never the case) and is stable, a feedforward controller is enough to reach the target. We write

$$u_d = F_u\, y_d, \tag{23}$$

$$x_d = F_x\, y_d, \tag{24}$$

where F_u and F_x are the feedforward gains corresponding to the input and state respectively. The total feedforward gain F depends on the matrices A, B, C, and K (explained in detailed in Sec. III C 2.

2. Linear quadratic regulator (LQR) design

The feedback control law links the input u to the state x by

$$u = u_d - K(x - x_d) = -Kx + Fy_d, \tag{25}$$

where K is the feedback control gain to be determined from control design and $F = F_u + KF_x$ is the total feedforward gain. Therefore, the resulting closed-loop system of Equations (20) and (21) can be written as

$$\begin{aligned} \dot{x} &= (A - BK)x + BFy_d, \\ y &= Cx. \end{aligned} \tag{26}$$

A standard linear control technique (linear-quadratic regulators)[40,41] is used in order to determine those gains K while minimizing a quadratic cost function.

3. Observer design

The feedback law (25) requires the knowledge of the full state x. However, in an actual experiment, we cannot measure the state directly; we measure only the outputs y. However, we may reconstruct an estimate of the state from the available sensor measurements using an *observer*. While running TRANSP simulations, we do have access to the full state, however, this will not be true for the real experiments, therefore we assume that our controller receive only five sensor measurements from TRANSP. The observer will then reconstruct the state estimate $\hat{x}$, with dynamics given by

$$\dot{\hat{x}} = A\hat{x} + Bu + L(y - C\hat{x}) = (A - LC)\hat{x} + Bu + Ly, \tag{27}$$

where the matrices A, B, and C are the same as those in the model (26), and L is a matrix of gains chosen such that the state estimate converges quickly relative to the system's dynamics. Using our linear model, we design an optimal observer (Kalman filter)[40,41] to find L.

The observer generates an estimate of the state from the physics model as represented by the state matrix, the inputs and outputs, and once combined to the feedback controller, it forms a linear quadratic Gaussian compensator.[40,41]

4. Integrator design

The goal is to track both the desired rotation profile and the thermal energy value (reference tracking). In order to do that, the steady state error between the output (measured) and the target profile has to be minimized by using an integrator and introducing a new state variable z that is the integral of the error

$$\dot{z} = y_d - y = y_d - Cx. \tag{28}$$

The new feedback law can be then written as

$$\begin{aligned} u &= \begin{pmatrix} -K & K_I \end{pmatrix} \begin{pmatrix} x \\ z \end{pmatrix} + Fy_d \\ &= u_d + K(x_d - x) + K_I \int (y_d - y), \end{aligned} \tag{29}$$

where K_I be the gain of the integrator.

5. Anti-windup design

A drawback of integral control is that if the actuator values are limited to some range as in our case, then the integrator can accumulate error when the actuator is "saturated," resulting in a poor transient performance, a phenomenon known as "integrator windup."

We use a standard anti-windup scheme[41,42] in which one feeds back the difference between the desired value of u and its actual (possibly saturated) value to eliminate this effect.

D. Study of robustness in stability and performance

We want to control system (20–21) to be able to reach the desired rotation profiles and stored energy (this is the role of the feedforward part of the controller) with good performance (this is the role of the feedback part of the controller), given the constraints we have on the actuators while ensuring closed-loop stability. This would be an easy task in the absence of any actuator limitations as system (20–21) does not present any fundamental limitations for control, so in theory, we could make the controller as fast as we want, at the expense of requiring huge actuator inputs. In practice, actuator saturation severely limits the possibilities for designing a controller exhibiting good performance, and saturation being a non-linear process, linear design tools cannot be used directly. So to design a controller with the best performance given these limitations, we start by ignoring the actuator saturation and building a fast and robust controller, then we subsequently consider the ramifications of realistic constraints on the actuators on the design until we get reasonable actuator inputs (they may saturate but only for a short time). This procedure ensures that we push performances near the top of what is achievable with the given actuator limitations.

Observer-based controllers, like Kalman filters, use an internal linear reduced-order model of the system which by its very nature cannot be 100% accurate. Furthermore, because of the lack of experimental data for NSTX-U, our model relies heavily on data from NSTX experiments so there is an increased risk that it might be inaccurate, that it might be missing some of the dynamics, or that some parameters might be off. These various inaccuracies, referred as *model uncertainty*, might make the closed-loop system

unstable or adversely affect its performance even though we designed the controller to be stable and fast. Fortunately it is possible to precisely describe this uncertainty, put proper bounds on it, and guarantee that our closed-loop system stays stable and meets all performance specifications in spite of it.

In this section, we design a nominal controller and define the performance specifications that should be maintained under parameter uncertainty. Then we show how to represent the system uncertainty resulting from parameter uncertainty, and we ensure that the controller previously designed offers robust stability and performance. Finally we consider the effect of actuator saturation while designing a final controller that works well in practice.

1. Nominal stability and performance

Designing a fast controller requires assigning large weights to the cost matrices of the LQR and the integrator, with caveats. Large weights on the output (instantaneous) errors generally not only lead to faster response times but also produce large inputs with fast variations. Large weights on the integrator can improve the settling time as the steady-state error is driven to zero faster, but they also tend to increase the overshoot and produce oscillations. Finding the perfect balance requires a fair amount of trial and error as one has to be careful not to introduce destabilizing oscillations. Since the model is uncertain, it is better to tune the Kalman filter to rely more on sensor measurements than on its internal model. The performance specifications are best expressed in terms of properties of the output sensitivity function S_o, in particular, its bandwidth, often defined as the smallest frequency to be transmitted, for which higher values means not only faster responses but also a higher sensitivity to noise, its peak value, which should be small for greater stability (a peak of less than 2, approximately 6 dB, is considered good), and its attenuation at steady-state (or at the lowest frequency considered). Since the duration of a plasma discharge is a few seconds, we only consider frequencies above 1 rad/s, and since we use a discrete-time controller (integrated into TRANSP), we only need to consider frequencies below the Nyquist frequency $\omega_N = \log(\pi/\Delta t)$ rad/s where Δt is our time step. To compute the sensitivity function, we need to split our controller into its *feedback* and *feedforward* parts, as shown in Figure 12, since the feedforward is irrelevant to the sensitivity. Note that F and K in this section are different from the F and K defined above. We have

$$S_o = (I + GK)^{-1}. \tag{30}$$

Ignoring actuator saturation, we can get very high theoretical performance by carefully assigning costs to the outputs and the integrator, and the weights of the Kalman filter.

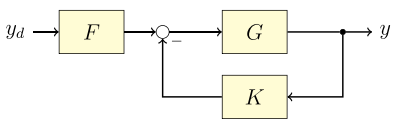

FIG. 12. Controller split into feedforward block (F) and feedback block (K).

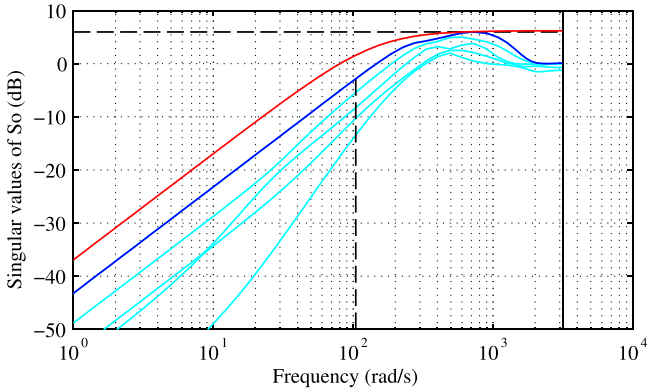

FIG. 13. Singular values of output sensitivity function for a fast controller designed ignoring actuator saturation. The dark blue line highlights the largest singular value. The red line is the upper bound corresponding to the performance specifications. The bandwidth is larger than 100 rad/s, the peak is smaller than 6 dB, and the attenuation at low frequencies is more than 40 dB.

Figure 13 shows the singular values of the output sensitivity function for a fast controller. The high bandwidth (above 100 rad/s) guarantees a short rise time while the limited peak value (less than 2) provides a good stability margin.

Figure 14 shows the outputs of the closed-loop system while tracking a target when this controller is used to control the linearized reduced system without actuator saturation. The target is reached in about 25 ms and there is no steady-state error. However, the inputs requested to achieve this

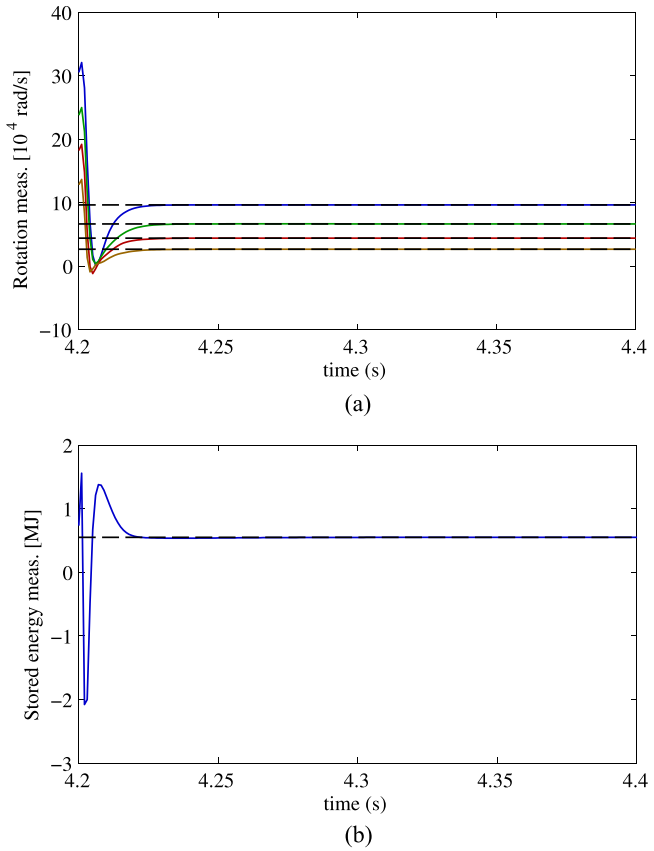

FIG. 14. Rotation measurements and stored energy over time while tracking a target for the linear system without actuator saturation. The target is reached in about 25 ms, and there is no steady-state error.

performance often exceed the saturation limits even in steady-state (Figure 15) because the integrator is working to bring the steady-state error to zero by requesting different inputs than those prescribed by the feedforward (which are within bounds). Note also that actuators are not constrained to minimal or maximal values, the beams and the coil current can become negative which is not a physically realistic solution.

We use this nominal controller as our reference for choosing performance specifications that must be met despite having uncertainty in the model. It is standard to encode these specifications in a weight W_P whose inverse forms an upper bound to the sensitivity function of the system. For simplicity, we choose W_P diagonal with all diagonal elements equal to the inverse of the upper bound of the largest singular value of the sensitivity function. The specifications are as follows: the bandwidth must be larger than 50 rad/s with a -20 dB/decade roll-off, and the peak of sensitivity must be less than 2 (6 dB). The corresponding upper bound for the sensitivity function is shown in red in Figure 13. The closed-loop system formed using our nominal controller is stable and meets these specifications so we can now address robustness.

2. Robust stability and performance

Next we want to introduce perturbations to our system. The concept of parameter uncertainty is thus

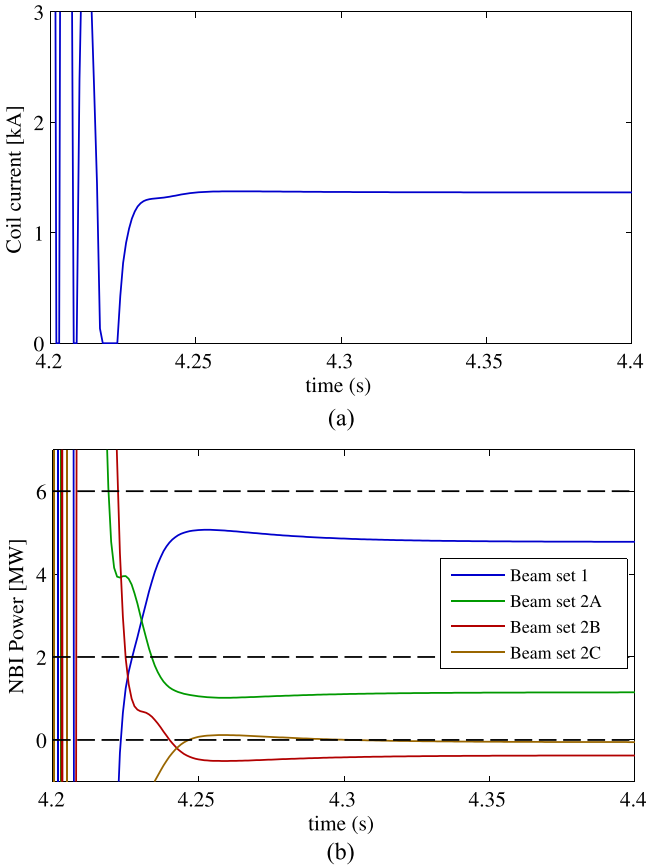

FIG. 15. Coil current and NBI power over time while tracking a target for the linear system without actuator saturation. The inputs requested often exceed the saturation limits, even in steady-state.

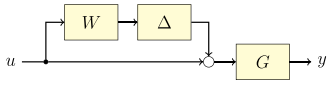

FIG. 16. Perturbed model $G_p = G(I + \Delta W)$.

introduced. The two parameters that are most likely to be varying significantly from their nominal value are χ_ϕ and τ_E. Let $\bar{\chi}_\phi$ be the nominal value (which depends on the radial variable ρ) of χ_ϕ, and let $\bar{\tau}_E$ be the nominal value of τ_E. We assume that the perturbed model G_p is built from perturbed values of the parameters $\chi_{\phi p}$ and τ_{Ep}, where $\chi_{\phi p}$ is a random perturbation of bounded magnitudes around $\bar{\chi}_\phi$ generated using 1D Perlin noise, and $\tau_{Ep} = \mu \cdot \bar{\tau}_E$ for some μ. Let Π be the set containing all such perturbed versions of our nominal model G. Robust stability (resp. performance) is obtained when all plants in Π are stable (resp. performant).

In order not to arbitrarily restrict the allowable magnitude of the perturbations, we start with a large range of allowed perturbations and progressively restrict the range until we get robust stability and performance.

To greatly simplify the analysis while being strictly conservative about stability and performance, we will use a *norm-bounded* description of uncertainty where Π is allowed to contain $\mathcal{H}_\infty$ norm-bounded perturbations of our nominal model G. To determine the best way to integrate this uncertainty into our model, we superimpose the Nyquist plots of many perturbed plants and we observe that right multiplicative uncertainty adequately represents the pattern we obtain. Thus we write

$$G_p = G(I + \Delta W), \tag{31}$$

where W is a weighting transfer function matrix, and Δ satisfies $||\Delta||_\infty < 1$. A block diagram of the perturbed plant is shown in Figure 16.

To find W, we first observe that $\Delta W = G^{-1}G_p - I$. Thus, since $||\Delta||_\infty < 1$, we can superimpose the Bode plots of $G^{-1}G_p - I$ for many perturbed plants and choose a low-order upper bound which will prescribe W. Note that $G^{-1}G_p - I$ and W are matrices so we must find upper bounds for each element.

Now equipped with a mathematical description of our perturbed system, we can address the robust stability. Using the block diagram algebra, we start by rearranging our system of Figure 17(a) into the $M\Delta$ configuration of Figure 17(b) to obtain the transfer function block matrix M

$$M = -WKS_oG. \tag{32}$$

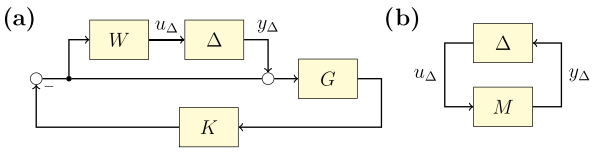

FIG. 17. Block diagrams of the loop of the perturbed closed-loop system stripped of all exogenous inputs and outputs. (a) Expanded system. (b) $M\Delta$ structure for robust stability analysis.

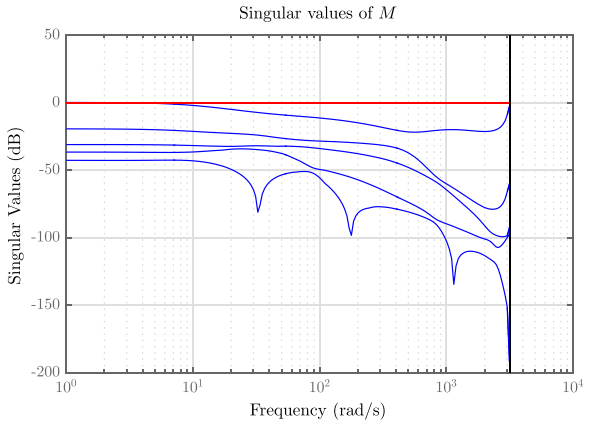

FIG. 18. Robust stability. The singular values of M are always less than 1.

When the nominal closed-loop system is stable and when the largest singular value of M is less than 1 for all frequencies, by theorem 8.4 of Ref. 40 (small-gain theorem), the closed-loop system is robustly stable. We found that with this very performant controller, we could achieve the robust stability for perturbations obtained from up to 10% variations of the nominal parameters (Figure 18). Controllers with less stringent performance requirements would allow even greater parameter variations (in the order of 50%).

To test for robust performance, we generate many perturbed plants and check that each one of them satisfies the performance specifications by superimposing the Bode plots of the largest singular value of all perturbed plants (Figure 19). We verify that our controller has a robust performance for the set of perturbed plants and the specifications stated above.

3. Actuator saturation

The controller studied above is fast at the expense of requiring not only large input values but also negative values which are impossible to produce in practice. Introducing actuator saturation without otherwise modifying the controller does not work as the large and oscillatory requested input values drive the actual inputs to constantly saturate one way or another which is particularly ineffective at controlling the system as can be seen in Figures 20 and 21.

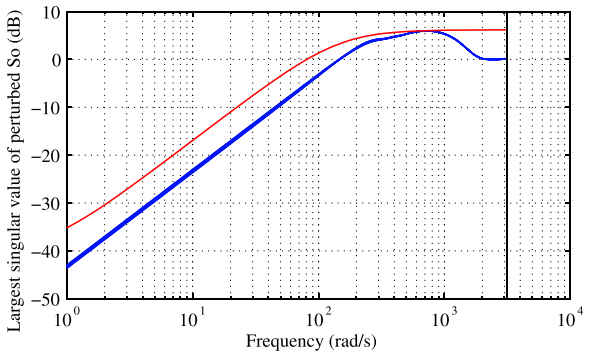

FIG. 19. Robust performance. The singular values of the transfer functions of 256 perturbed plants are shown superimposed in blue. All perturbed transfer functions meet the performance specifications indicated by the upper bound in red.

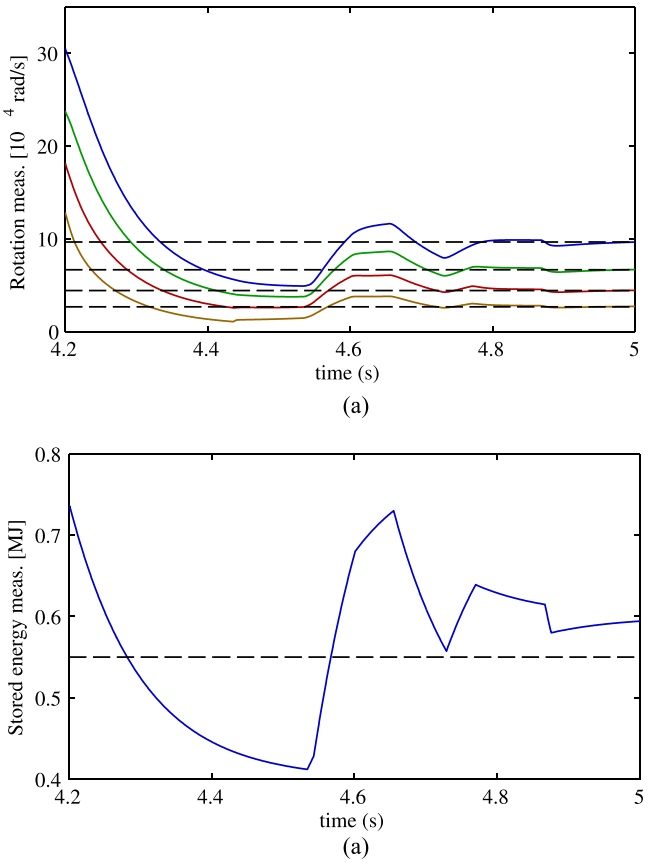

FIG. 20. Rotation measurements and stored energy over time while tracking a target with actuator saturation and the nominal controller designed above. The time response is erratic because the controller is requesting too large inputs that saturate.

So instead we progressively reduce the weights assigned to the cost function until the input values get within reasonable bounds such that saturation only occurs for short durations, which allows us to obtain the best controller we can design in practice. Note that since the saturation process is non-linear, we can no longer rely on linear control design tools like putting an upper bound on the sensitivity function for specifying performance specifications so we have to rely on time responses of the closed-loop system. The closed-loop system exhibits a fast response time for sensor measurements (Figure 22) while only saturating the inputs for a short time after a command is received (Figure 23). However, the time response for the stored energy is slower than for the rotation measurements, and the target is not perfectly reached. This is a design choice made to improve the tracking of the rotation at the expense of the stored energy. Indeed, Equation (3) imposes a trade-off between the stored energy and the beam powers by removing one degree of freedom on how the controller can set the inputs making it impossible to simultaneously and efficiently track both the rotation and the energy.

As shown in Sec. IV C, this controller works well in practice despite the additional burden of the full actuator constraints (saturation, Pulse Width Modulation (PWM), limited on/off switches, refractory period) and the fact the actual system to be controlled is non-linear.

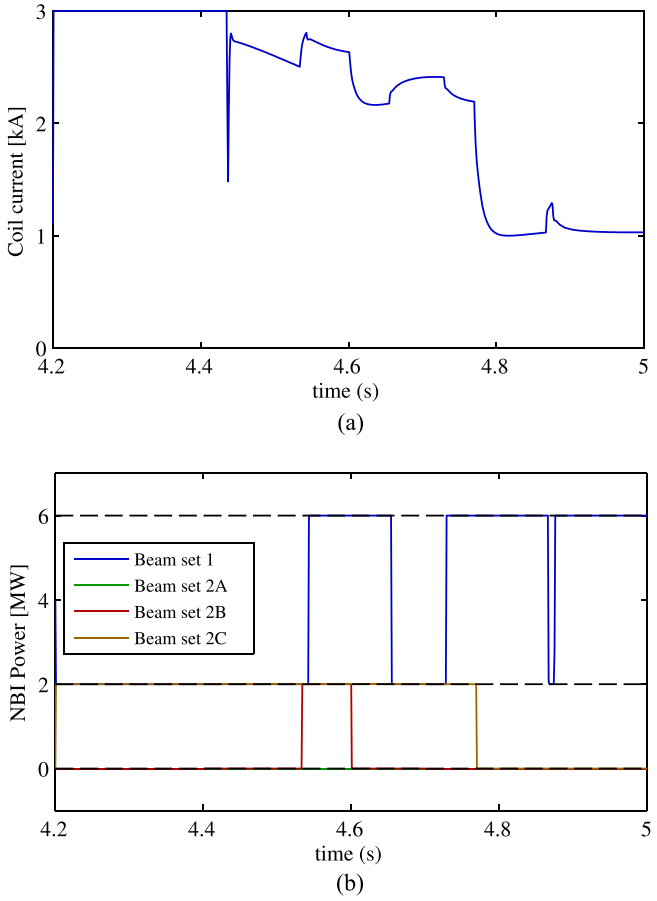

FIG. 21. Coil current and NBI power over time while tracking a target with actuator saturation and the nominal controller designed above. The beam powers are constantly saturating and sometimes jumping between their upper and lower limit.

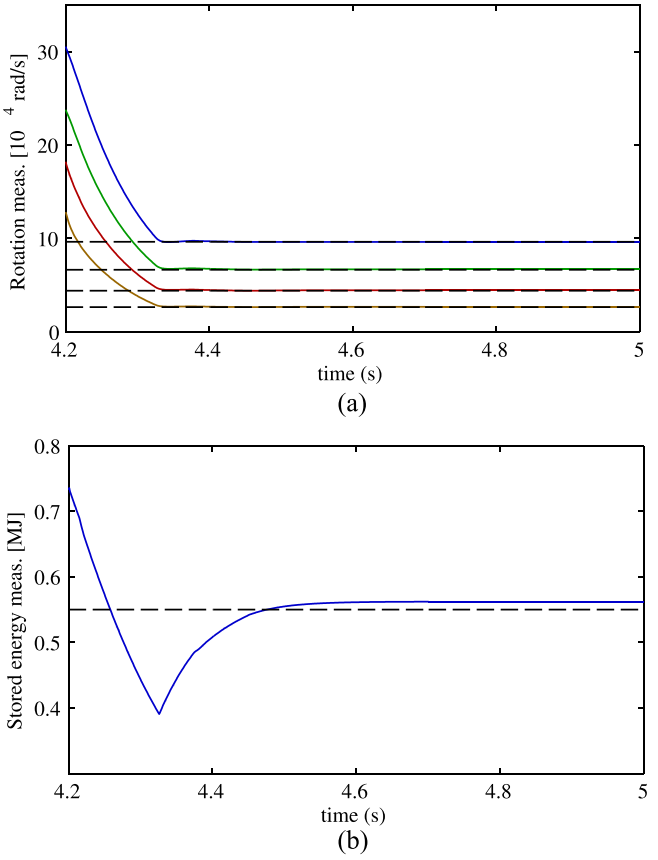

FIG. 22. Rotation measurements and stored energy over time while tracking a target with actuator saturation and a controller designed to account for it. By design, the response is slower for the stored energy and the target is not perfectly reached.

IV. SIMULATION RESULTS

The goal of the simulations is to test the controller on both a higher fidelity model (TRANSP) as well as the simplified reduced-order model. The desired profiles shown in Figures 24 will track the targets in both cases, and the results will be presented to see the effectiveness of the controller.

A. Actuator constraints

Like in the NSTX device, the two different actuators (NTV coil current and NBI beam power) have constraints that need to be taken into account when applied on the device (NSTX-U) through TRANSP. These constraints are made for the safety of the operations, they reflect the practicability and the feasibility of some requests to the device. The constraints will be added to the dynamics equations through restrictions on the actuators of the controller.

Due to the sufficiently low inductance of the circuit, the coil current response is much faster than the dynamics. The restriction is only a limitation of its value between 0 and 3000 A (no lag is assumed between the controller action and its application).

For the NBI actuators in NSTX-U, each of the 6 beams has to be treated individually. Fusing the three beams of the first set was just a simplification in our model but because we apply the controller on TRANSP, each beam is coded separately, and each beam can either be on and produce 2 MW of power or off and produce 0 MW. In addition, each beam can only be switched off a maximum of 20 times per plasma discharge to prevent device fatigue issues, and there is a refractory period of 10 ms after each switch on or off during which the beam cannot be switched again. Also, due to diagnostic considerations, one NBI source is typically always on, and so the overall sum of the injected power is considered to be between 2 and 12 MW.

These physical restrictions constrain the model and controller to be discrete and to use Pulse Width Modulation (PWM) for each beam power actuator in order to obtain the requested control values between 2 and 12 MW.

B. Computational approach (TRANSP implementation)

To predict the toroidal rotation and the stored energy for NSTX-U, TRANSP is run in a predictive mode for a given set of beam powers and coil current. It also takes as input models for the plasma boundary shape, plasma current, electron and ion (Chang-Hinton model[43]) temperature and density profiles and the momentum diffusivity coefficient.

The actuator commands required for closed-loop rotation and stored energy control simulations are entered into TRANSP, which serves as a plasma simulator for testing the

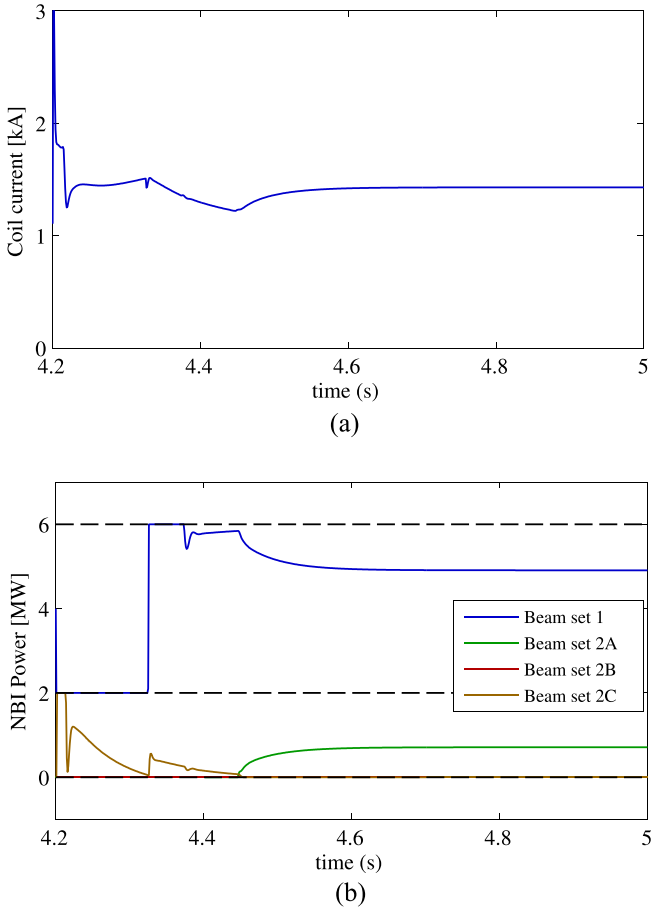

FIG. 23. Coil current and NBI power over time while tracking a target with actuator saturation and a controller designed to account for it. Saturation only occurs for short periods during the transient.

present controller. For more details on the TRANSP implementation, see Boyer *et al.*[15]

C. Simulation on TRANSP

The discretized controller is now applied to both the reduced-order model and the TRANSP predictive model, considering all the constraints listed in Section IV A for all the actuators, and instead of applying the exact beam powers numerical value as requested by the controller, each of the 6 beams will be modulated individually while satisfying

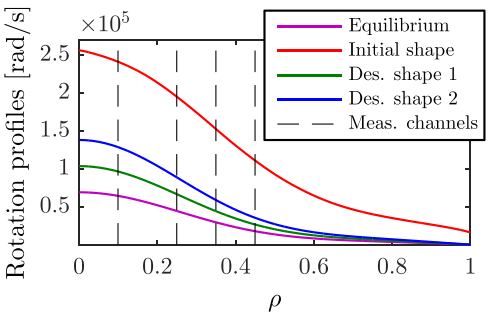

FIG. 24. Rotation profiles: definition of the initial profile, equilibrium profile w_0 used for the linearization and the desired profiles to reach w_d. The measurement points r are the intersections of the different profiles with the measurement channels.

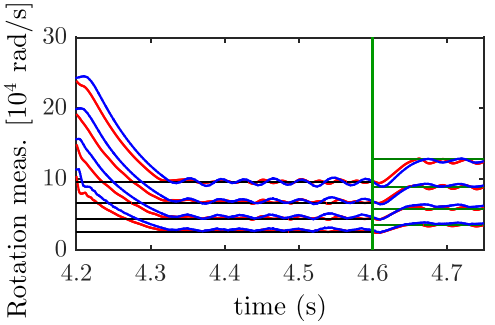

FIG. 25. Comparison of the rotation measurements when PWM is applied for both the reduced-order model (red lines) and the TRANSP predictive model (blue lines).

all the constraints. The upper bound for the coil current is 3000 A.

At the beginning of each duty cycle, the controller sets the requested power. During the duty cycle, the beams switch on and off at most once to minimize the number of switches. Because of the 10 ms refractory period and the limited switches, the exact requested power cannot always be met.

The longer the duty cycle, the better for the device because it means less command switches so less fatigue, but a longer duration introduces a longer controller lag which impairs performance. A duration smaller than the refractory period is chosen for the duty cycle (6 ms).

Figure 25 compares the rotation measurements when the PWM controller is applied to both the reduced-order model and the TRANSP predictive model in order to reach two targets, one at $t = 4.2$ s, and the other starting at $t = 4.6$ s. Before $t = 4.2$ s, both models are not controlled (open loop).

Figure 26 represents the corresponding TRANSP predictive stored energy measurement. At $t = 4.2$ s, a target of 0.55 MJ is reached then at $t = 4.6$ s another target of 0.65 MJ is reached.

The oscillations in both figures are due to the modulations that occur on each of the beam power source. The different beam power sources are represented in Figure 27(b), and the corresponding coil current in Figure 27(a).

When at $t = 4.2$ s, we close the loop, the coil current saturates immediately to enable the rotation profile to drop quickly from its high initial state (all beams on) to the first desired rotation profile, and then compensates for when the beam power is too high in order to decrease both the toroidal

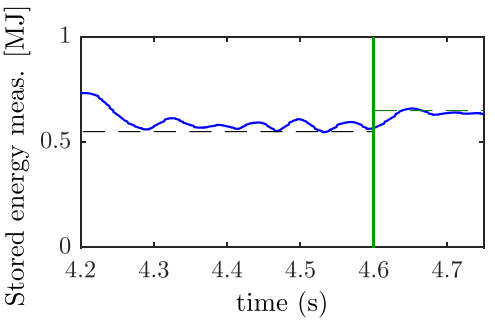

FIG. 26. Stored energy measurements when PWM is applied for the TRANSP predictive model (blue line).

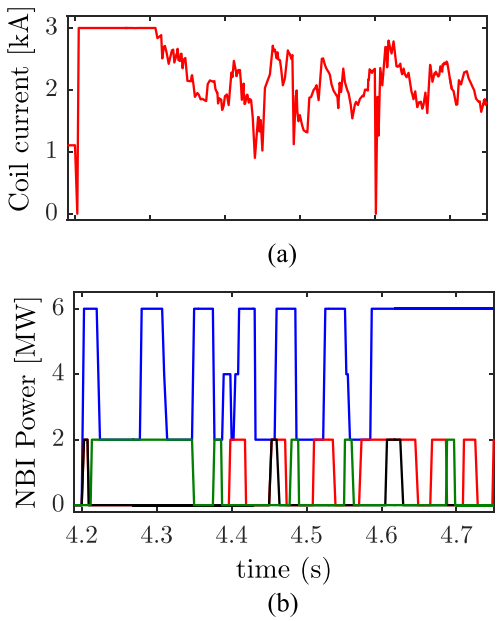

FIG. 27. Time evolution of the coil current and the beam power.

rotation and the stored energy and thus limits the overshoot. We thus reach the desired rotation and energy targets within the momentum diffusion time (0.1 s).

The resulting measurements are very oscillatory but their amplitudes are damped and measurements from the reduced-order model are very close to those from TRANSP which again shows that the simplified model gives us a good qualitative approximation of the TRANSP rotation and energy prediction model.

V. CONCLUSIONS AND FUTURE WORK

Reduced-order model based feedback control applied to plasma physics problems is not just a simple application of known engineering methods of flow control to a new domain. Plasma is a complex fluid within an electromagnetic field that requires high dimensional non linear models. It is becoming crucial when building fusion devices to use and rely intensively on these modeling and control design tools since these very important predictive methods are necessary to help planning the adequate most stable design and help suppressing the instabilities that can occur and grow and become a major problem that can break and compromise the device.

Simple reduced-order models have been developed to capture simultaneously the rotational toroidal momentum balance and the stored energy in NSTX-U device. These models utilize the neutral beam injections and the neoclassical toroidal viscosity. The outputs from these models have been compared with numerical results from a predictive model of NSTX-U and were found to be in good agreement. Based on these simplified models, a linear "model-based" controller of the plasma toroidal rotation and stored energy has been developed using optimal control techniques. These reduced-order controllers were then tested using the NSTX-U predictive model and enabled the rotation profile and stored energy to reach some desired profiles and value.

This paper studies the full theoretical design of controllers that can serve multiple purposes, but the study will be complete if a direct application of this type of controllers on NSTX-U device is possible. The Plasma Control System (PCS) that controls the plasma has been upgraded to include rotation control. Next step of testing the rotation control and stored energy control can soon become a reality. Real time control might reveal unforeseen complications which can alter the dynamics predicted by these models and force a revision and update of the design by adding new constraints, for instance.

Another important design consideration is to take into account the influence that multiple controllers with different goals can have on each other: toroidal rotation or stored energy is not the only quantities that must be controlled during a plasma discharge. Current or shape control must be considered too, as well as other quantities depending on the purpose of each experimental run. Therefore many actuators controlled by different controllers may have to operate at the same time, and some of these actuators can influence or delay others and prevent some controllers from reaching their goals. Therefore having an overview of all the actuators included into the system is important and would be a very interesting problem to examine. This would enable us to clarify what the possible combinations of controllers are that do not compete with each other, but instead work towards compatible objectives.

Finally, an important design consideration for both fusion devices and its various controllers is the positioning of the actuators and sensors. In every study or application of localized feedback control (through actuators and sensors), the designer must decide where the actuators and sensors should physically be placed. Few studies in control applications have rigorously analyzed where the actuator and sensor locations are most effective, and what are the implications of its placement on the dynamics and the controller. A large number of studies simply guess or sometimes choose purposefully or randomly the locations without any deep analysis. The placement of actuators and sensors can be just as important as the controller design itself since there are fundamental limitations which can make a system almost impossible to control due to poor placement of actuators and sensors. In plasma physics, we are usually constrained to use the diagnostic device locations as they were placed originally in the machine. Moving these would cause technical hassles that technicians would be reluctant to do. It can also be impossible to change the location as it can be a part of the device design. Therefore it is crucial to study the optimal location of the actuators-sensors for rotation control and take this into account during the design phase of next-generation fusion devices.

ACKNOWLEDGMENTS

This work was supported by the U.S. Department of Energy under Contract No. DE-AC02-09CH11466 and U.S. Department of Energy Grant No. DE-FG02-99ER54524.

[1]J. Menard, S. Gerhardt, M. Bell, J. Bialek, A. Brooks, J. Canik, J. Chrzanowski, M. Denault, L. Dudek, D. Gates, N. Gorelenkov, W. Guttenfelder, R. Hatcher, J. Hosea, R. Kaita, S. Kaye, C. Kessel, E. Kolemen, H. Kugel, R. Maingi, M. Mardenfeld, D. Mueller, B. Nelson, C. Neumeyer, M. Ono, E. Perry, R. Ramakrishnan, R. Raman, Y. Ren, S.

Sabbagh, M. Smith, V. Soukhanovskii, T. Stevenson, R. Strykowsky, D. Stutman, G. Taylor, P. Titus, K. Tresemer, K. Tritz, M. Viola, M. Williams, R. Woolley, H. Yuh, H. Zhang, Y. Zhai, A. Zolfaghari, and NSTX Team, Nucl. Fusion **52**, 083015 (2012).
[2]M. Ono, S. Kaye, Y.-K. Peng, G. Barnes, W. Blanchard, M. Carter, J. Chrzanowski, L. Dudek, R. Ewig, D. Gates, R. Hatcher, T. Jarboe, S. Jardin, D. Johnson, R. Kaita, M. Kalish, C. Kessel, H. Kugel, R. Maingi, R. Majeski, J. Manickam, B. McCormack, J. Menard, D. Mueller, B. Nelson, B. Nelson, C. Neumeyer, G. Oliaro, F. Paoletti, R. Parsells, E. Perry, N. Pomphrey, S. Ramakrishnan, R. Raman, G. Rewoldt, J. Robinson, A. Roquemore, P. Ryan, S. Sabbagh, D. Swain, E. Synakowski, M. Viola, M. Williams, J. Wilson, and NSTX Team, Nucl. Fusion **40**, 557 (2000).
[3]Y.-K. M. Peng, P. J. Fogarty, T. W. Burgess, D. J. Strickler, B. E. Nelson, J. Tsai, C. A. Neumeyer, R. Bell, C. Kessel, J. Menard, D. Gates, B. LeBlanc, D. Mikkelsen, E. Fredrickson, L. Grisham, J. Schmidt, P. Rutherford, S. Sabbagh, A. Field, A. Sykes, I. Cook, O. Mitarai, and Y. Takase, Plasma Phys. Controlled Fusion **47**, B263 (2005).
[4]Y. K. M. Peng, Fusion Science and Technology **60**(2), 441–448 (2011).
[5]Y. Peng, T. Burgess, A. Carroll, C. Neumeyer, J. Canik, M. Cole, W. Dorland, P. Fogarty, L. Grisham, D. Hillis, Y. Katoh, K. Korsah, M. Kotschenreuther, R. LaHaye, S. Mahajan, R. Majeski, B. Nelson, B. Patton, D. Rasmussen, S. Sabbagh, A. Sontag, R. Stoller, C.-C. Tsai, P. Valanju, J. Wagner, and G. Yoder, Fusion Sci. Technol. **56**(2), 957 (2009).
[6]D. Gates, J. Menard, R. Maingi, S. Kaye, S. Sabbagh, S. Diem, J. Wilson, M. Bell, R. Bell, J. Ferron, E. Fredrickson, C. Kessel, B. LeBlanc, F. Levinton, J. Manickam, D. Mueller, R. Raman, T. Stevenson, D. Stutman, G. Taylor, K. Tritz, H. Yu, and NSTX Research Team, Nucl. Fusion **47**, 1376 (2007).
[7]J. Menard, M. Bell, R. Bell, S. Bernabei, J. Bialek, T. Biewer, W. Blanchard, J. Boedo, C. Bush, M. Carter, W. Choe, N. Crocker, D. Darrow, W. Davis, L. Delgado-Aparicio, S. Diem, C. Domier, D. D'Ippolito, J. Ferron, A. Field, J. Foley, E. Fredrickson, D. Gates, T. Gibney, R. Harvey, R. Hatcher, W. Heidbrink, K. Hill, J. Hosea, T. Jarboe, D. Johnson, R. Kaita, S. Kaye, C. Kessel, S. Kubota, H. Kugel, J. Lawson, B. LeBlanc, K. Lee, F. Levinton, N. C. Luhmann, Jr., R. Maingi, R. Majeski, J. Manickam, D. Mansfield, R. Maqueda, R. Marsala, D. Mastrovito, T. Mau, E. Mazzucato, S. Medley, H. Meyer, D. Mikkelsen, D. Mueller, T. Munsat, J. Myra, B. Nelson, C. Neumeyer, N. Nishino, M. Ono, H. Park, W. Park, S. Paul, T. Peebles, M. Peng, C. Phillips, A. Pigarov, R. Pinsker, A. Ram, S. Ramakrishnan, R. Raman, D. Rasmussen, M. Redi, M. Rensink, G. Rewoldt, J. Robinson, P. Roney, A. Roquemore, E. Ruskov, P. Ryan, S. Sabbagh, H. Schneider, C. Skinner, D. Smith, A. Sontag, V. Soukhanovskii, T. Stevenson, D. Stotler, B. Stratton, D. Stutman, D. Swain, E. Synakowski, Y. Takase, G. Taylor, K. Tritz, A. von Halle, M. Wade, R. White, J. Wilgen, M. Williams, J. Wilson, H. Yuh, L. Zakharov, W. Zhu, S. Zweben, R. Akers, P. Beiersdorfer, R. Betti, T. Bigelow, M. Bitter, P. Bonoli, C. Bourdelle, C. Chang, J. Chrzanowski, L. Dudek, P. Efthimion, M. Finkenthal, E. Fredd, G. Fu, A. Glasser, R. Goldston, N. Greenough, L. Grisham, N. Gorelenkov, L. Guazzotto, R. Hawryluk, J. Hogan, W. Houlberg, D. Humphreys, F. Jaeger, M. Kalish, S. Krasheninnikov, L. Lao, J. Lawrence, J. Leuer, D. Liu, G. Oliaro, D. Pacella, R. Parsells, M. Schaffer, I. Semenov, K. Shaing, M. Shapiro, K. Shinohara, P. Sichta, X. Tang, R. Vero, M. Walker, and W. Wampler, Nucl. Fusion **47**, S645 (2007).
[8]D. Gates, J. Ahn, J. Allain, R. Andre, R. Bastasz, M. Bell, R. Bell, E. Belova, J. Berkery, R. Betti, J. Bialek, T. Biewer, T. Bigelow, M. Bitter, J. Boedo, P. Bonoli, A. Boozer, D. Brennan, J. Breslau, D. Brower, C. Bush, J. Canik, G. Caravelli, M. Carter, J. Caughman, C. Chang, W. Choe, N. Crocker, D. Darrow, L. Delgado-Aparicio, S. Diem, D. D'Ippolito, C. Domier, W. Dorland, P. Efthimion, A. Ejiri, N. Ershov, T. Evans, E. Feibush, M. Fenstermacher, J. Ferron, M. Finkenthal, J. Foley, R. Frazin, E. Fredrickson, G. Fu, H. Funaba, S. Gerhardt, A. Glasser, N. Gorelenkov, L. Grisham, T. Hahm, R. Harvey, A. Hassanein, W. Heidbrink, K. Hill, J. Hillesheim, D. Hillis, Y. Hirooka, J. Hosea, B. Hu, D. Humphreys, T. Idehara, K. Indireshkumar, A. Ishida, F. Jaeger, T. Jarboe, S. Jardin, M. Jaworski, H. Ji, H. Jung, R. Kaita, J. Kallman, O. Katsuro-Hopkins, K. Kawahata, E. Kawamori, S. Kaye, C. Kessel, J. Kim, H. Kimura, E. Kolemen, S. Krasheninnikov, P. Krstic, S. Ku, S. Kubota, H. Kugel, R. L. Haye, L. Lao, B. LeBlanc, W. Lee, K. Lee, J. Leuer, F. Levinton, Y. Liang, D. Liu, N. Luhmann, Jr., R. Maingi, R. Majeski, J. Manickam, D. Mansfield, R. Maqueda, E. Mazzucato, D. McCune, B. McGeehan, G. McKee, S. Medley, J. Menard, M. Menon, H. Meyer, D. Mikkelsen, G. Miloshevsky, O. Mitarai, D. Mueller, S. Mueller, T. Munsat, J. Myra, Y. Nagayama, B. Nelson, X. Nguyen, N. Nishino, M. Nishiura, R. Nygren, M. Ono, T. Osborne, D. Pacella, H. Park, J. Park, S. Paul, W. Peebles, B. Penaflor, M. Peng, C. Phillips, A. Pigarov, M. Podesta, J. Preinhaelter, A. Ram, R. Raman, D. Rasmussen, A. Redd, H. Reimerdes, G. Rewoldt, P. Ross, C. Rowley, E. Ruskov, D. Russell, D. Ruzic, P. Ryan, S. Sabbagh, M. Schaffer, E. Schuster, S. Scott, K. Shaing, P. Sharpe, V. Shevchenko, K. Shinohara, V. Sizyuk, C. Skinner, A. Smirnov, D. Smith, S. Smith, P. Snyder, W. Solomon, A. Sontag, V. Soukhanovskii, T. Stoltzfus-Dueck, D. Stotler, T. Strait, B. Stratton, D. Stutman, R. Takahashi, Y. Takase, N. Tamura, X. Tang, G. Taylor, C. Taylor, C. Ticos, K. Tritz, D. Tsarouhas, A. Turrnbull, G. Tynan, M. Ulrickson, M. Umansky, J. Urban, E. Utergberg, M. Walker, W. Wampler, J. Wang, W. Wang, A. Welander, J. Whaley, R. White, J. Wilgen, R. Wilson, K. Wong, J. Wright, Z. Xia, X. Xu, D. Youchison, G. Yu, H. Yuh, L. Zakharov, D. Zemlyanov, and S. Zweben, Nucl. Fusion **49**, 104016 (2009).
[9]S. Gerhardt, D. Gates, S. Kaye, R. Maingi, J. Menard, S. Sabbagh, V. Soukhanovskii, M. Bell, R. Bell, J. Canik, E. Fredrickson, R. Kaita, E. Kolemen, H. Kugel, B. L. Blanc, D. Mastrovito, D. Mueller, and H. Yuh, Nucl. Fusion **51**, 073031 (2011).
[10]R. Buttery, R. Akers, E. Arends, N. Conway, G. Counsell, G. Cunningham, C. Gimblett, M. Gryaznevich, R. Hastie, M. Hole, I. Lehane, R. Martin, A. Patel, T. Pinfold, O. Sauter, D. Taylor, G. Turri, M. Valovic, M. Walsh, H. Wilson, and MAST team, Nucl. Fusion **44**, 1027 (2004).
[11]I. Chapman, W. Cooper, J. Graves, M. Gryaznevich, R. Hastie, T. Hender, D. Howell, M.-D. Hua, G. Huysmans, D. Keeling, Y. Liu, H. Meyer, C. Michael, S. Pinches, S. Saarelma, S. Sabbagh, and MAST Team, Nuclear Fusion **51**, 073040 (2011).
[12]S. Gerhardt, D. Mastrovito, M. Bell, M. Cropper, D. Gates, E. Kolemen, J. Lawson, B. Marsala, J. Menard, D. Mueller, and T. Stevenson, Fusion Sci. Technol. **61**(1), 11 (2012).
[13]D. Gates, J. Ferron, M. Bell, T. Gibney, R. Johnson, R. Marsala, D. Mastrovito, J. Menard, D. Mueller, B. Penaflor, S. Sabbagh, and T. Stevenson, Nucl. Fusion **46**, 17 (2006).
[14]E. Kolemen, D. Gates, S. Gerhardt, R. Kaita, H. Kugel, D. Mueller, C. Rowley, and V. Soukhanovskii, Nucl. Fusion **51**, 113024 (2011).
[15]M. Boyer, R. Andre, D. Gates, S. Gerhardt, I. Goumiri, and J. Menard, Nucl. Fusion **55**, 053033 (2015).
[16]I. Goumiri, C. Rowley, S. Sabbagh, D. Gates, S. Gerhardt, M. Boyer, R. Andre, E. Kolemen, and K. Taira, Nucl. Fusion **56**, 036023 (2016).
[17]E. Kolemen, D. Gates, C. Rowley, N. Kasdin, J. Kallman, S. Gerhardt, V. Soukhanovskii, and D. Mueller, Nucl. Fusion **50**, 105010 (2010).
[18]K. Erickson, D. Gates, S. Gerhardt, J. Lawson, R. Mozulay, P. Sichta, and G. Tchilinguirian, Fusion Eng. Des. **89**, 853 (2014).
[19]S. Gerhardt, D. Brennan, R. Buttery, R. L. Haye, S. Sabbagh, E. Strait, M. Bell, R. Bell, E. Fredrickson, D. Gates, B. LeBlanc, J. Menard, D. Stutman, K. Tritz, and H. Yuh, Nucl. Fusion **49**, 032003 (2009).
[20]Y. Park, S. Sabbagh, J. Bialek, J. Berkery, S. Lee, W. Ko, J. Bak, Y. Jeon, J. Park, J. Kim, S. Hahn, J.-W. Ahn, S. Yoon, K. Lee, M. Choi, G. Yun, H. Park, K.-I. You, Y. Bae, Y. Oh, W.-C. Kim, and J. Kwak, Nucl. Fusion **53**, 083029 (2013).
[21]S. Sabbagh, J. Berkery, R. Bell, J. Bialek, S. Gerhardt, J. Menard, R. Betti, D. Gates, B. Hu, O. Katsuro-Hopkins, B. LeBlanc, F. Levinton, J. Manickam, K. Tritz, and H. Yuh, Nucl. Fusion **50**, 025020 (2010).
[22]J. W. Berkery, S. A. Sabbagh, R. Betti, B. Hu, R. E. Bell, S. P. Gerhardt, J. Manickam, and K. Tritz, Phys. Rev. Lett. **104**, 035003 (2010).
[23]A. Garofalo, E. Strait, L. Johnson, R. La Haye, E. Lazarus, G. Navratil, M. Okabayashi, J. Scoville, T. Taylor, and A. Turnbull, Phys. Rev. Lett. **89**, 235001 (2002).
[24]E. J. Strait, Phys. Plasmas **1**, 1415–1431 (1994).
[25]G. Campbell, J. Ferron, E. Mckee, A. Nerem, T. Smith, C. Greenfield, R. Pinsker, and E. Lazarus, "New DIII-D tokamak plasma control system," presented at the 17th Symposium on Fusion Technology, Rome (Italy), 14–18 Sep. 1992 (Vol. 1, pp. 14–18).
[26]J. Lawson, M. Bell, R. Marsala, and D. Mueller, "Beta normal control of TFTR using fuzzy logic," In Fusion technology 1994. Proceedings. Vol. 1.
[27]N. Zornig, "Experimental results using the JET real time power control system," Jt. Eur. Torus - Publ. 155–160 (1996).
[28]T. Oikawa, K. Tsuchiya, K. Kurihara, Y. Kawamata, T. Fukuda, T. Fujita, and Y. Neyatani, Fusion Eng. Des. **70**, 175 (2004).
[29]J. Scoville, D. Humphreys, J. Ferron, and P. Gohil, in *Proceedings of the 24th Symposium on Fusion Technology SOFT-24*; [Fusion Eng. Des. **82**, 1045 (2007)].
[30]R. Budny, Nucl. Fusion **34**, 1247 (1994).
[31]R. Goldston, D. McCune, H. Towner, S. Davis, R. Hawryluk, and G. Schmidt, J. Comput. Phys. **43**, 61 (1981).

[32]J. R. Goldston, in *Proceedings of the Course and Workshop Varenna* (1986), Vol. 1, p. 165.
[33]J. Callen, A. Cole, and C. Hegna, Nucl. Fusion **49**, 085021 (2009).
[34]ITER Physics Expert Group on Confinement and Transport, ITER Physics Expert Group on Confinement Modelling, Database, and ITER Physics Basis Editors, Nucl. Fusion **39**, 2175 (1999).
[35]S. Kaye, M. Bell, R. Bell, E. Fredrickson, B. LeBlanc, K. Lee, S. Lynch, and S. Sabbagh, Nucl. Fusion **46**, 848 (2006).
[36]K. Shaing, K. Ida, and S. Sabbagh, Nucl. Fusion **55**, 125001 (2015).
[37]W. Zhu, S. A. Sabbagh, R. E. Bell, J. M. Bialek, M. G. Bell, B. P. LeBlanc, S. M. Kaye, F. M. Levinton, J. E. Menard, K. C. Shaing, A. C. Sontag, and H. Yuh, Phys. Rev. Lett. **96**, 225002 (2006).
[38]M. Grant and S. Boyd, CVX: Matlab Software for Disciplined Convex Programming, Version 2.1, 2014.
[39]M. Grant and S. Boyd, in *Recent Advances in Learning and Control*, Lecture Notes in Control and Information Sciences, edited by V. Blondel, S. Boyd, and H. Kimura (Springer-Verlag Limited, 2008), pp. 95–110.
[40]S. Skogestad and I. Postlethwaite, *Multivariable Feedback Control: Analysis and Design* (John Wiley & Sons, 2005).
[41]K. J. Astrom and R. M. Murray, *Feedback Systems: An Introduction for Scientists and Engineers* (Princeton University Press, 2008).
[42]B. L. Stevens and F. L. Lewis, *Aircraft Control and Simulation* (John Wiley & Sons, 2003).
[43]C. S. Chang and F. L. Hinton, Phys. Fluids **25**, 1493 (1982).